

Preparation of reduced graphene oxide decorated with Cu-Co Oxide Electrode and its application for Sensitive Determination of Nitrite in Food Samples

Jing xi Ma^{1,*}, Yue Ning¹, Liu Yang¹, Yin Feng², Yan Liu^{2,*}

¹ College of Food Science and Engineering, Changchun University, Chang'Chun 130012, China

² School of Life Sciences, Changchun SCI-TECH University, ChangChun 130000, China

*E-mail: majingxi1981@sina.com, yangliu811981@163.com

Received: 6 September 2021 / Accepted: 14 October 2021 / Published: 10 November 2021

This study was focused on the electrochemical determination of nitrite in food samples using reduced graphene oxide decorated with Cu-Co oxide nanoparticles (Cu-Co oxide NPs) on a glassy carbon electrode (Cu-Co oxide/rGO/GCE). An electrodeposition technique was used for the modification of the GCE surface with rGO and decoration of the rGO nanosheets with Cu-Co oxide NPs. Morphological and structural analyses using SEM and XRD revealed that rGO nanosheets were electrodeposited on GCE in a typical crumpled and slightly curved structure which provided more active defect sites and a high specific surface area for high porous electrodeposition of Cu-Co oxide NPs. The electrochemical studies using the CV and DPV techniques showed that Cu-Co oxide/rGO/GCE exhibited a sensitive, stable, and selective response to nitrite because of the synergetic effect of Cu-Co oxide NPs and rGO, and the sensitivity, limit of detection and linear range of Cu-Co oxide/rGO/GCE to determination of nitrite were obtained at 0.07436 $\mu\text{A}/\mu\text{M}$, 0.04 μM and 100 to 2800 μM , respectively. The practicability of Cu-Co oxide/rGO/GCE was investigated in the determination of the nitrite in ham sausage sample, and the results exhibited acceptable values for recoveries (97.42 to 98.65%) and RSDs (3.55 to 4.23%) for the detection of nitrite, indicating to great precision and accuracy in the determination of nitrite content in food samples.

Keywords: Electrodeposition; Cu-Co oxide nanoparticles; reduced graphene oxide; Nitrite; Food samples

1. INTRODUCTION

The nitrite (NO_2^-) is widely used as an inorganic fertilizer, explosive, as an oxidizing agent in chemical and pharmaceutical industries, and as preservatives in food industry especially to cure meats such as beef, pork, sausage, bacon and salami [1, 2]. Nitrites give cured meats their distinct color, aroma and flavor, and they are responsible for the characteristic pink color of cured meats [3]. In

addition, nitrite prevents the growth of a harmful bacterium called *Clostridium botulinum* and it may also have preservation effects on other harmful and spoilage bacteria [4, 5].

The presence of nitrite ions in water samples and human food product sources can cause health effects such as increased heart rate, nausea, headaches, and abdominal cramps [6-8]. High dietary intake of nitrite can increase the production of N-nitroso compounds which are suspected to cause stomach cancer [9, 10]. Elevated levels of nitrite in the blood can react with ferrous (Fe^{2+}) hemoglobin, which leads to methemoglobinemia and decreases the capacity of oxygen transport [11, 12]. The World Health Organization's studies have shown that there is sufficient evidence that processed meats cause cancer, particularly colon cancer, and processed meats were classified as carcinogenic to humans [13, 14]. Accordingly, some regulations have been established on the acceptable daily intake of food additives [15, 16].

Therefore, it is necessary to determine the nitrite level in the food industry, and many studies have been performed for identification and determination of the nitrite using spectrophotometry, fluorometry, electrochemiluminescent, chemiluminescent flow-injection analysis, liquid chromatography, capillary electrophoresis and electrochemical methods [17-21]. Among them, the potential low-cost, and ease of operation and portability of electrochemical analysis tools offer a number of attractive options for the on-site analysis of food, drugs and industrial wastewater. Moreover, the modified electrodes with suitable nanostructured and hybrid catalysts not only enhance electrochemical response but also improve the selectivity and linear range in analytical analyses. Therefore, this study was focused on the electrochemical determination of nitrite in food samples using reduced graphene oxide decorated with Cu-Co oxide nanoparticles on a glassy carbon electrode.

2. MATERIALS AND METHOD

2.1. Modification the GCE

The GCE surface was decorated with CuO NPs, Co_3O_4 NPs, Cu-Co oxide NPs, rGO and Cu-Co oxide NPs /rGO. Before the electrodeposition, surface of GCE was gently polished with alumina slurries (99.99%, 0.05-0.3 μm , Sigma-Aldrich) on a polishing pad and rinsed with deionized water and ethanol (>99%, Merck, Germany). The electroposition was carried out via a potentiostat/galvanostat electrochemical workstation (model CS350, Wuhan Corrtest Instruments Corp., Ltd., China) using a conventional electrochemical cell which contained a working electrode (GCE), a reference electrode (Ag/AgCl/Saturated KCl), and an auxiliary electrode (platinum plate). For electrodeposition of rGO nanosheets on GCE, the electrochemical deposition was accomplished in 1.0 g/l rGO (>99.3wt%, 1-12 μm , Luoyang Tongrun Info Technology Co., Ltd., China) in 0.1M phosphate buffer solution (PBS) pH 8.5 at a potential range of -1.2 V to +0.6 V at a scan rate of 15mV/s for 10 minutes [22]. Electrodeposition of Cu-Co oxide NPs on GCE or rGO/GCE was conducted at potential of -1.2 V for 4 minutes in the electrolyte solution containing a mixture of 10ml of 0.5M $\text{CuCl}_2 \cdot 5\text{H}_2\text{O}$ (99.9%, Sigma-Aldrich), 10ml of 0.5M $\text{CoCl}_2 \cdot 6\text{H}_2\text{O}$ ($\geq 99\%$, Sigma-Aldrich) and 70ml of 1M NH_4Cl (>99%, Sigma-Aldrich) [23].

2.2. Real sample preparation

For preparation of the real sample of ham sausage, the ham sausage samples were purchased from a local market. The ham sausage were weighed, and 1 kg of ham sausages was minced and added to 1l deionized water at 75 °C, and stirred for 10 minutes. The mixture rested in the fridge overnight. Then, the mixture was stirred again for 15 minutes. After then, the mixture was filtered. The resultant liquid was transported to centrifuge tubes (1000 rpm for 5 minutes). Finally, the achieved supernatants were mixed with 0.1 M PBS solution in an equal volume ratio.

2.3. Characterization

Cyclic voltammetry (CV) and differential pulse voltammetry (DPV) experiments were also carried out by the potentiostat/galvanostat electrochemical workstation. The electrolytes for electrochemical analyses were $K_3[Fe(CN)_6]$ (99.5%, Sinoconvoy new material (Shan Dong) Co., Ltd., China) containing 0.1 M KCl (99.5%, (>99%, Merck, Germany), and 0.1M PBS, which was produced from 0.1M NaH_2PO_4 and 0.1M Na_2HPO_4 in equal volume ratio. The morphologies of the nanostructure modified surface of electrodes were characterized by scanning electron microscopy (SEM, JSM-5510LV, JEOL Ltd., Tokyo, Japan). X-ray diffractometer (XRD, PaNalytical Pro X'Pert Pro., Almelo, The Netherlands) was used to study the structural properties of modified electrodes.

3. RESULTS AND DISCUSSION

3.1. Structural analyses of modified electrodes

The SEM images of the morphologies of the nanostructured surface of electrodes are presented in Figure 1. The SEM images of Figures 1a, 1b and 1c clearly display the successful electrodeposition of CuO NPs, Co_3O_4 NPs and Cu–Co oxide NPs on GCE surface, respectively. The CuO NPs, Co_3O_4 NPs and Cu–Co oxide NPs were electrodeposited in a spherical shape with an average diameter of ~ 110, 97 and 82 nm, respectively. As observed, some of the nanoparticles are irregular in shape or in contact with their neighbors. CuO NPs and Co_3O_4 NPs have larger sizes than the bimetallic oxide nanoparticles which can be related to more nucleation and crystal growth of CuO NPs and Co_3O_4 NPs [24]. Figure 1d shows the rGO nanosheets electrodeposited on GCE which have a typical crumpled and slightly curved structure, some of which are wrinkled together. Figure 1e shows the CuO–Co NPs decorated on the rGO/GCE surface. As seen, the crumpled and wrinkled structure of nanosheets can provide more active defect sites and a high specific surface area for high porous electrodeposition of metallic nanoparticles [25]. The well-dispersed bimetallic nanoparticles on rGO nanosheets are electrodeposited with a diameter of ~ 80 nm. Therefore, the small size and high porous structure of Cu–Co oxide/rGO/GCE, plus the higher specific surface area of Cu–Co oxide NPs and rGO can provide more effective reaction sites for absorption of analyses which facilitate the electron transfer and improve electrocatalytic activity [26].

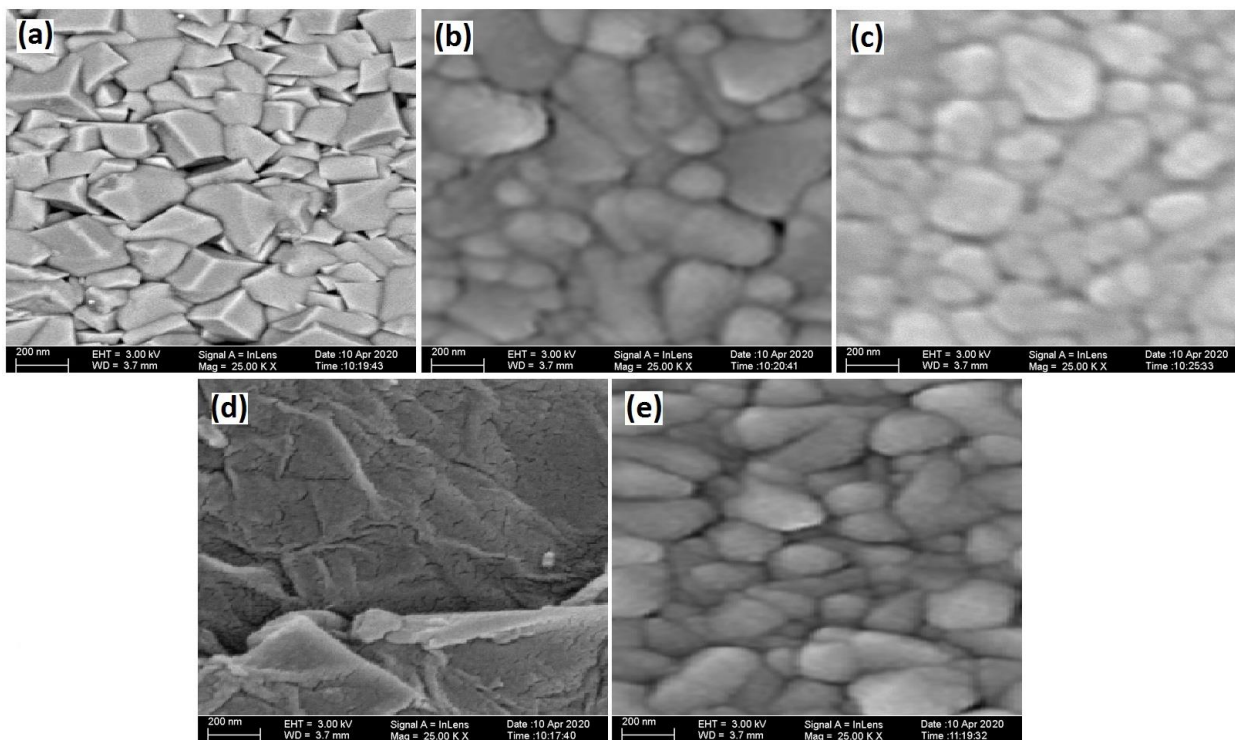


Figure 1. The SEM images of surface of (a) CuO/GCE, (b) Co₃O₄/GCE, (c) Cu–Co oxide/GCE, (d) rGO/GCE and (e) Cu–Co oxide NPs/rGO/GCE.

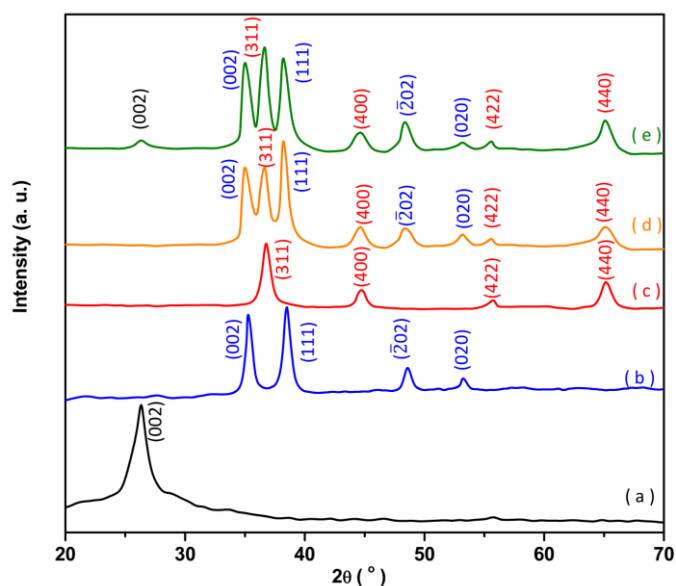


Figure 2. XRD pattern of electroposited (a) rGO, (b) CuO NPs, (c) Co₃O₄ NPs, (d) Cu–Co oxide NPs and (e) Cu–Co oxide NPs/rGO

Fig. 2 shows the XRD analyses of electroposited rGO, CuO NPs, Co₃O₄ NPs, Cu–Co oxide NPs, rGO and Cu–Co oxide NPs/rGO on GCE. The XRD patterns of rGO in Fig. 1a display a single peak at 26.26° that corresponds to the (002) graphitic lattice plane of rGO. As observed from Figure 2b, there are diffraction peaks at 35.16°, 38.41°, 48.59° and 53.29° which are assigned to (002), (111), ($\bar{2}$ 02), and (020) planes, indicating the growth of the monoclinic structure of CuO (JCPDS Card

No. 80-1917). It is observed from Figure 2c that the XRD pattern of Co_3O_4 NPs shows the diffraction peaks at 36.69° , 44.65° , 55.51° and 65.17° which are related to (311), (400), (422), and (440) planes of the monoclinic structure of Co_3O_4 (JCPDS card No. 00-042-1467). Figures 2d and 2e exhibit the XRD pattern of Cu–Co oxide NPs and Cu–Co oxide NPs/rGO. These patterns contain all of the diffraction patterns of Co_3O_4 and CuO, indicating the crystal growth of bimetallic oxide in the electrodeposition process. Moreover, the Cu–Co oxide NPs/rGO show the peak plane of (002) related to rGO, corresponding to the successful electrodeposition of Cu–Co oxide NPs on the rGO/GCE surface.

3.1. Electrochemical analyses

Figure 3 displays the CV responses of GCE, rGO/GCE, CuO/GCE, Co_3O_4 /GCE, Cu–Co oxide/GCE, rGO/GCE and Cu–Co oxide/rGO/GCE in 0.5 mM $\text{K}_3[\text{Fe}(\text{CN})_6]$ containing the 0.1 M KCl at the scan rate of 15 mV/s. The pair of well-defined redox peaks of 0.26 and 0.21 V are observed for all electrodes, correlating with the quasi-reversible redox reaction of $[\text{Fe}(\text{CN})_6]^{3-/4-}$ [27]. A comparison between the GCE and rGO/GCE reveals that the rGO significantly increases the electrochemical response of modified electrodes. This improvement is attributed to rGO porous nanosheets, high surface area and excellent electrical conductivity [28, 29]. Comparison between the CuO/GCE, Co_3O_4 /GCE, Cu–Co oxide/GCE also illustrates that metal oxide nanoparticles can enhance the electrochemical response due to high conductivity, great surface area and small dimensional size [30].

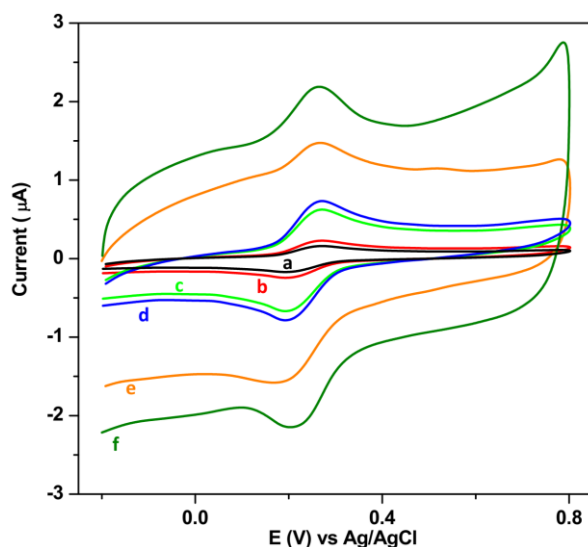
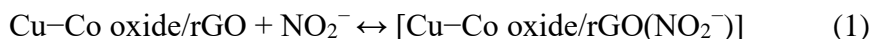


Figure 3. The CV responses of (a) GCE, (b) rGO/GCE, (c) CuO/GCE, (d) Co_3O_4 /GCE, (e) Cu–Co oxide/GCE, rGO/GCE and (f) Cu–Co oxide/rGO/GCE in 0.5 mM $\text{K}_3[\text{Fe}(\text{CN})_6]$ containing the 0.1 M KCl at the scan rate of 15 mV/s.

Cu–Co oxide/GCE and CuO/GCE have higher peak currents than Co_3O_4 /GCE due to CuO's high electrical conductivity [31]. As seen from the CV response of Cu–Co oxide/rGO/GCE, there is further enhancement of the electrochemical response that is related to the formation of the carbon

hybrid structure through the combination of rGO and metal oxide nanoparticles, improving the electrical conductivity and electrochemical redox properties. Therefore, the decoration of rGO nanosheets with Cu–Co oxide NPs promotes the electron transfer rate that is compatible with SEM studies.

Figure 4 shows the DPV responses of bare and modified GCE in 0.1M PBS pH 7 at a scan rate of 50mV/s in the presence of 50 μ M nitrite. As seen, the GCE displays a negligible oxidation peak current at 0.92 V in response to 50 μ M nitrite. The DPV plots of rGO/GCE, CuO/GCE, Co₃O₄/GCE, Cu–Co oxide/GCE and Cu–Co oxide/rGO/GCE display the oxidation peak currents of 0.90 V, 0.91 V, 0.74V, 0.73V and 0.74 V, respectively. Competition between the DPV responses demonstrates to higher electrocatalytic response of Cu–Co oxide/rGO/GCE to detection of nitrite which is associated with the great surface area formed by the decoration of Cu–Co oxide nanoparticles on rGO/GCE that provides the numerous active sites for adsorption of molecules of analytes. Moreover, the incorporation of Co₃O₄ nanoparticles on CuO and rGO hybrid structures leads to a decrease the oxidation potential Also, rGO increases the oxidation peak current [32, 33]. According to the following mechanism [34, 35], the synergistic effect of Cu–Co oxide nanoparticles and rGO can effectively catalyze nitrite oxidation:



It is indicated by the interaction between Cu–Co oxide/rGO and nitrite which results in the complex of [Cu–Co oxide/rGO(NO₂⁻)] (reaction (1)). It is followed by the formation of NO₂ through the loss of one electron (reaction (2)).

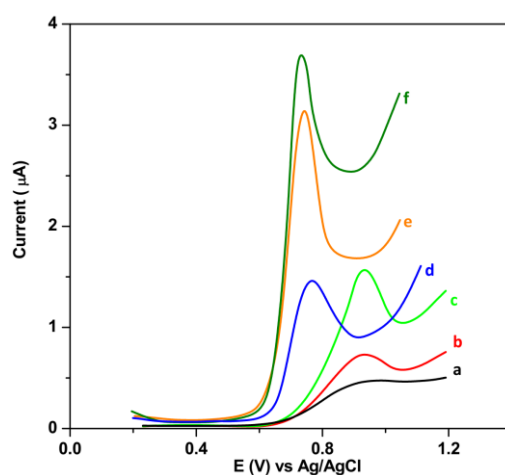


Figure 4. DPV responses of (a) GCE, (b) rGO/GCE, (c) CuO/GCE, (d) Co₃O₄/GCE, (e) Cu–Co oxide/GCE, rGO/GCE and (f) Cu–Co oxide/rGO/GCE in 0.1M PBS at a 50mV/s scan rate in existence of 50 μ M nitrite.

Finally, NO_2 is converted to NO_2^- and NO_3^- (reactions (3) and (4)). Thus, the Cu–Co oxide/rGO/GCE was used for the results of electrochemical studies.

Figure 5 depicts the DPV response and resultant calibration graph of Cu–Co oxide/rGO/GCE to successive additions of nitrite in 0.1M PBS at a 50mV/s scan rate in the presence of 50 μM nitrite. It can be found that the oxidation peak current was linearly improved with the rise of the nitrite content in the electrochemical cell. The resulted calibration plot shows that the linear range, limit of detection and sensitivity of Cu–Co oxide/rGO/GCE to determination of nitrite are obtained from 100 to 2800 μM , 0.04 μM and 0.07436 $\mu\text{A}/\mu\text{M}$, respectively. Furthermore, the sensing properties of Cu–Co oxide/rGO/GCE are compared with different electrochemical nitrite sensors in Table 1 which indicate comparable or better sensing properties of Cu–Co oxide/rGO/GCE than other nitrite electrochemical sensors. Moreover, rGO is mainly composed of a sp^2 hybridized carbon framework that includes the hydroxyl ($-\text{OH}$), quinone ($\text{C}=\text{O}$), carboxy ($-\text{COOH}$), or epoxide ($-\text{O}-$) groups which interact through hydrogen bonding with the polar metal-oxide surface [36]. As a consequence, it provides good chemical stability and high mechanical strength which can enhance the linear range of Cu–Co oxide/rGO/GCE which can be the advantages of this study.

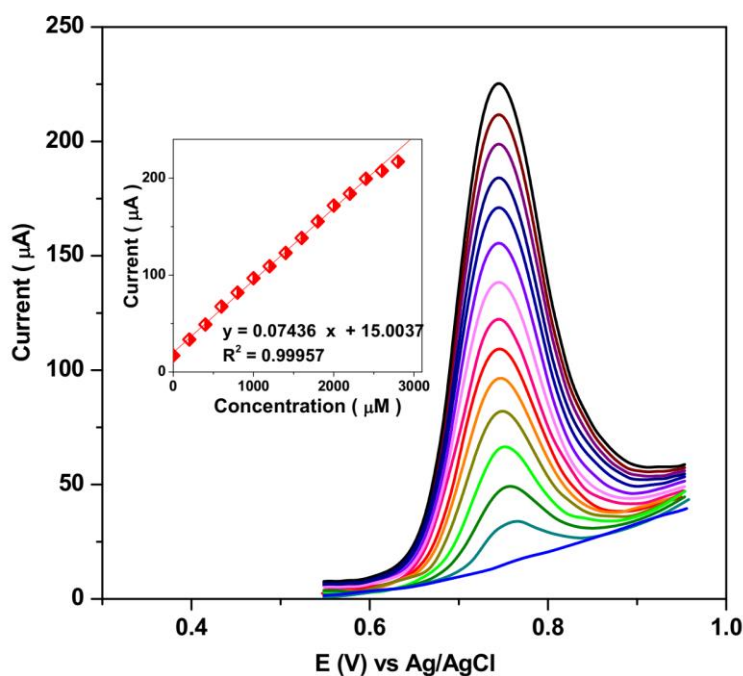


Figure 5. DPV response and resulted calibration graph of Cu–Co oxide/rGO/GCE to successive addition of 200 μM nitrite in 0.1M PBS at a 50mV/s scan rate.

The anti-interference capability and selectivity of Cu–Co oxide/rGO/GCE were investigated through the study of the effects of common interfering species in nitrite determination. Table 2 shows the results of DPVs analysis in 0.1M PBS with the addition 10 μM of nitrite and 100 μM of interfering species. Results show that addition of 100 μM of ascorbic acid causes considerable interference in the determination of nitrite using Cu–Co oxide/rGO/GCE which is agreement with the report of Thomas et al. [37] for determination the nitrite using [5,10,15,20-tetrakis (4-methoxyphenyl) porphyrinato]

manganese (III) chloride modified gold electrode. Furthermore, no obvious interference effect in the determination of nitrite was observed after the addition of 100 M of Fe^{3+} , Ca^{2+} , Mg^{2+} , Cu^{2+} , K^+ , PO_4^{2-} , CO_3^{2-} , SO_4^{2-} , NO_3^- and glucose, indicating that the proposed sensor can be used as selective electrochemical sensor for determination of nitrite.

Table 1. A comparison between the sensing properties of Cu–Co oxide/rGO/GCE with with different electrochemical nitrite sensors.

| Electrodes | Method | Detection limit(μM) | Linear range(μM) | Ref. |
|---|--------|----------------------------------|-------------------------------|-----------|
| Cu–Co oxide/rGO/GCE | DPV | 0.04 | 100–2800 | This work |
| Cu-Co-Prussian Blue analogue /MWCNTs/GCE | DPV | 0.5 | 400–2100 | [38] |
| Graphene– tetrasodium 1,3,6,8-pyrenetetrasulfonic acid – Mb/GCE | CV | 10 | 50–2500 | [39] |
| Au/polyaniline/carbon paste electrode | CV | 25 | 38– 1000 | [40] |
| AgNP/GCE | AMP | 1.2 | 10–1000 | [41] |
| Fe_2O_3 /MWCNTs/GCE | AMP | 0.1 | 10–1000 | [42] |
| Ag NPs/MWCNTs/GCE | AMP | 0.095 | 1–100 | [43] |
| Pt NPs/Au/GCE | AMP | 5 | 10–1000 | [44] |
| Cu/MWCNTs/GCE | AMP | 1.8 | 5–1260 | [45] |
| Naphthylethylenediamine/Au electrode | EIS | 0.02 | 0.1–4 | [46] |

Table 2. Results of DPVs analysis of Cu–Co oxide/rGO/GCE in 0.1 M PBS pH 7 to addition 10 μM of nitrite and 100 μM of interfering species.

| Specie | Concentration(μM) | Electro-catalytic peak currents at 0.75 V (μA) | RSD* (%) |
|--------------------|--------------------------------|---|--------------|
| Fe^{3+} | 10 | 0.7441 | ± 0.0045 |
| Ca^{2+} | 100 | 0.0701 | ± 0.0013 |
| Mg^{2+} | 100 | 0.0871 | ± 0.0009 |
| Cu^{2+} | 100 | 0.0933 | ± 0.0011 |
| K^+ | 100 | 0.0589 | ± 0.0117 |
| PO_4^{2-} | 100 | 0.0101 | ± 0.0035 |
| CO_3^{2-} | 100 | 0.0889 | ± 0.0013 |
| SO_4^{2-} | 100 | 0.0911 | ± 0.0022 |
| NO_3^- | 100 | 0.0350 | ± 0.0018 |
| Glucose | 100 | 0.0773 | ± 0.0025 |
| Ascorbic acid | 100 | 0.3771 | ± 0.0077 |

* Relative standard deviation

In order to study the practicability of Cu–Co oxide/rGO/GCE in determining the nitrite in food samples, the nitrite content was detected in the ham sausage sample using the DPV analysis in real sample in a 0.1M PBS at a 50mV/s scan rate with additions of nitrite solution. Fig. 6 shows the DPV

measurements and the resulting calibration plot of prepared real samples. It can be found from the calibration plot that the nitrite concentration in the electrochemical cell of prepared specimens of the ham sausage in 0.1M PBS was 69.1 mg/l, implying the presence of 138.2 mg of nitrite in 1 kg of ham sausage. This value is very close to the reported nitrite concentration in ham sausage (150 mg/kg) [47]. Moreover, Table 3 presents the results of standard addition experiments. Results exhibited the acceptable values for recoveries (97.42 to 98.65%) and RSDs (3.55 to 4.23%) for detection of nitrite using Cu–Co oxide/rGO/GCE, indicating great precision and accuracy in determining nitrite content in food samples.

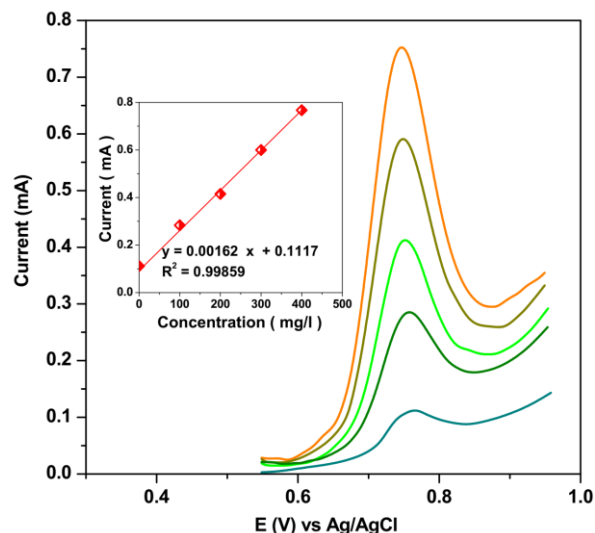


Figure 6. DPV measurements and resulted calibrations plot of Cu–Co oxide/rGO/GCE in real samples of ham sausage in 0.1M PBS at 50mV/s scan rate with additions of nitrite solution.

Table 3. Results of standard addition experiments for determination of nitrite in the prepared real sample of ham sausage (n = 4).

| Added(mg/l) | Found(mg/l) | RSD(%) | Recovery(%) |
|-------------|-------------|--------|-------------|
| 100.0 | 97.8 | 3.55 | 97.80 |
| 200.0 | 197.3 | 3.67 | 98.65 |
| 300.0 | 295.8 | 4.23 | 98.60 |
| 400.0 | 389.7 | 4.10 | 97.42 |

4. CONCLUSION

This study was carried out for synthesis and electrochemical studies of Cu–Co oxide/rGO/GCE as for determination of nitrite in food samples. The electrodeposition technique was used for the modification of the GCE surface by rGO and decoration of the rGO nanosheets Cu–Co oxide NPs. The structural analyses revealed that rGO nanosheets were electrodeposited on GCE in a typical crumpled and slightly curved structure and Cu–Co oxide NPs successfully electrodeposited on rGO nanosheets.

The electrochemical studies showed that Cu–Co oxide/rGO/GCE exhibited a sensitive, stable and selective response to nitrite, and the sensitivity, limit of detection and linear range of Cu–Co oxide/rGO/GCE to determination of nitrite were obtained at $0.07436\mu\text{A}/\mu\text{M}$, $0.04\mu\text{M}$ and 100 to $2800\mu\text{M}$, respectively. The results of the study on the practicability of Cu–Co oxide/rGO/GCE in the determination of the nitrite in ham sausage sample exhibited the acceptable values for recoveries and RSDs for detection of nitrite, indicating great precision and accuracy in determining nitrite content in food samples.

References

1. J. DU, Q.-h. WANG and L.-q. LIU, *Food Science and Technology*, 8 (2007) 1.
2. F. Shahidi and R.B. Pegg, *Food Chemistry*, 43 (1992) 185.
3. Y. Orooji, B. Tanhaei, A. Ayati, S.H. Tabrizi, M. Alizadeh, F.F. Bamoharram, F. Karimi, S. Salmanpour, J. Rouhi and S. Afshar, *Chemosphere*, 281 (2021) 130795.
4. M.P. Dutra, G. de Cássia Aleixo, A.d.L.S. Ramos, M.H.L. Silva, M.T. Pereira, R.H. Piccoli and E.M. Ramos, *Radiation Physics and Chemistry*, 119 (2016) 125.
5. Y. Liu, B. Jiang, L. Zhao, L. Zhao, Q. Wang, C. Wang and B. Xu, *Spectrochimica Acta Part A: Molecular and Biomolecular Spectroscopy*, 261 (2021) 120009.
6. W.-Y. Huang, G.-Q. Wang, W.-H. Li, T.-T. Li, G.-J. Ji, S.-C. Ren, M. Jiang, L. Yan, H.-T. Tang and Y.-M. Pan, *Chem*, 6 (2020) 2300.
7. H. Karimi-Maleh, Y. Orooji, F. Karimi, M. Alizadeh, M. Baghayeri, J. Rouhi, S. Tajik, H. Beitollahi, S. Agarwal and V.K. Gupta, *Biosensors and Bioelectronics*, 184 (2021) 113252.
8. Y. Orooji, P.N. Asrami, H. Beitollahi, S. Tajik, M. Alizadeh, S. Salmanpour, M. Baghayeri, J. Rouhi, A.L. Sanati and F. Karimi, *Journal of Food Measurement and Characterization*, (2021) 1.
9. Y. Yu, Y. Zhao, Y.-L. Qiao, Y. Feng, W.-L. Li and W.-D. Fei, *Journal of Materials Science & Technology*, 84 (2021) 10.
10. H. Karimi-Maleh, M.L. Yola, N. Atar, Y. Orooji, F. Karimi, P.S. Kumar, J. Rouhi and M. Baghayeri, *Journal of colloid and interface science*, 592 (2021) 174.
11. V.Y. Titov and Y.M. Petrenko, *Biochemistry (Moscow)*, 70 (2005) 473.
12. Q. Zhang, Y. Ding, S. Gu, S. Zhu, X. Zhou and Y. Ding, *Food Research International*, 137 (2020) 109339.
13. J.J. Sindelar and A.L. Milkowski, *Nitric oxide*, 26 (2012) 259.
14. H. Karimi-Maleh, S. Ranjbari, B. Tanhaei, A. Ayati, Y. Orooji, M. Alizadeh, F. Karimi, S. Salmanpour, J. Rouhi and M. Sillanpää, *Environmental Research*, 195 (2021) 110809.
15. C. Xue, J. You, H. Zhang, S. Xiong, T. Yin and Q. Huang, *Food Chemistry*, 363 (2021) 130304.
16. X. Yangli, M. Liuwei, C. Xiaojing, C. Xi, S. Laijin, Y. Leiming, S. Wen and G. Huang, *Plasma Science and Technology*, 23 (2021) 085503.
17. Q.-H. Wang, L.-J. Yu, Y. Liu, L. Lin, R.-g. Lu, J.-p. Zhu, L. He and Z.-L. Lu, *Talanta*, 165 (2017) 709.
18. P. Singh, M.K. Singh, Y.R. Beg and G.R. Nishad, *Talanta*, 191 (2019) 364.
19. A. Salimi, A. Noorbakhash and F.S. Karonian, *International Journal of Electrochemical Science*, 1 (2006) 435.
20. H. Xu, J. Peng, M. Zhu and J. Liu, *International Journal of Electrochemical Science*, 12 (2017) 10642.

21. H. Karimi-Maleh, M. Alizadeh, Y. Orooji, F. Karimi, M. Baghayeri, J. Rouhi, S. Tajik, H. Beitollahi, S. Agarwal and V.K. Gupta, *Industrial & Engineering Chemistry Research*, 60 (2021) 816.
22. L. Chen, Y. Tang, K. Wang, C. Liu and S. Luo, *Electrochemistry communications*, 13 (2011) 133.
23. K. Justice Babu, S. Sheet, Y.S. Lee and G. Gnana Kumar, *ACS Sustainable Chemistry & Engineering*, 6 (2018) 1909.
24. G. Li, W. Zhang, N. Luo, Z. Xue, Q. Hu, W. Zeng and J. Xu, *Nanomaterials*, 11 (2021) 1926.
25. R. Kumar, R. Savu, R.K. Singh, E. Joanni, D.P. Singh, V.S. Tiwari, A.R. Vaz, E.T. da Silva, J.R. Maluta and L.T. Kubota, *Carbon*, 117 (2017) 137.
26. Q. He, Y. Wu, Y. Tian, G. Li, J. Liu, P. Deng and D. Chen, *Nanomaterials*, 9 (2019) 115.
27. S. Phetsang, P. Kidkhunthod, N. Chanlek, J. Jakmune, P. Mungkornasawakul and K. Ounnunkad, *Scientific reports*, 11 (2021) 1.
28. C.B. Ching, J. Abdullah and N.A. Yusof, *Journal of Sensors*, 2021 (2021) 1.
29. H. Karimi-Maleh, Y. Orooji, A. Ayati, S. Qanbari, B. Tanhaei, F. Karimi, M. Alizadeh, J. Rouhi, L. Fu and M. Sillanpää, *Journal of Molecular Liquids*, 329 (2021) 115062.
30. N. Gao, J. Yu, Q. Tian, J. Shi, M. Zhang, S. Chen and L. Zang, *Chemosensors*, 9 (2021) 79.
31. A.R. Ansari, S.A. Ansari, N. Parveen, M.O. Ansari and Z. Osman, *Materials*, 14 (2021) 5032.
32. E.F. Aboelfetoh, A.A. Elhelaly and A.H. Gemeay, *Journal of environmental chemical engineering*, 6 (2018) 623.
33. A.V. Munde, B.B. Mulik, R.P. Dighole and B.R. Sathe, *New Journal of Chemistry*, 44 (2020) 15776.
34. Y. Ma, X. Song, X. Ge, H. Zhang, G. Wang, Y. Zhang and H. Zhao, *Journal of Materials Chemistry A*, 5 (2017) 4726.
35. L. Fu, S. Yu, L. Thompson and A. Yu, *RSC Advances*, 5 (2015) 40111.
36. B. Gupta, N. Kumar, K. Panda, V. Kanan, S. Joshi and I. Visoly-Fisher, *Scientific Reports*, 7 (2017) 45030.
37. D. Thomas, L. Rajith, L. Lonappan, S. Issac and K.G. Kumar, *Food Analytical Methods*, 5 (2012) 752.
38. L. Hong-Ying, W. Jia-Jun, Z.-H. HUANG, M. Huan, X. Han-Xiao, Q. Yu-Bin, Z. Wei-Jie and G. Chun-Chuan, *Chinese Journal of Analytical Chemistry*, 47 (2019) e19066.
39. R. Yue, Q. Lu and Y. Zhou, *Biosensors and Bioelectronics*, 26 (2011) 4436.
40. M. Etesami, N.S. Chandran, M.H. Hussin, A. Ripin, R. Adnan, A.N.A. Sujari and N. Mohamed, *International Journal of Electrochemical Science*, 11 (2016) 8332.
41. Z. Wang, F. Liao, T. Guo, S. Yang and C. Zeng, *Journal of Electroanalytical Chemistry*, 664 (2012) 135.
42. X.R. Lin, Y.F. Zheng and X.C. Song, *Bulletin of Materials Science*, 41 (2018) 1.
43. Y. Wan, Y.F. Zheng, H.T. Wan, H.Y. Yin and X.C. Song, *Food Control*, 73 (2017) 1507.
44. P. Miao, M. Shen, L. Ning, G. Chen and Y. Yin, *Analytical and bioanalytical chemistry*, 399 (2011) 2407.
45. D. Manoj, R. Saravanan, J. Santhanalakshmi, S. Agarwal, V.K. Gupta and R. Boukherroub, *Sensors and Actuators B: Chemical*, 266 (2018) 873.
46. Z. Wang, X. Liu, M. Yang, S. An, X. Han, W. Zhao, Z. Ji, X. Zhao, N. Xia and X. Yang, *International Journal of Electrochemical Science*, 9 (2014) 1139.
47. M. Cantwell and C. Elliott, *J. Clin. Nutr. Diet*, 3 (2017) 27.